Theses and Dissertations

August 2016

Phase Sensitive Thermography of Magnetostrictive Materials Under Periodic Excitations

Peng Yang
University of Wisconsin-Milwaukee

Follow this and additional works at: https://dc.uwm.edu/etd

Part of the Condensed Matter Physics Commons, Materials Science and Engineering Commons, and the Optics Commons

PHASE SENSITIVE THERMOGRAPHY OF MAGNETOSTRICTIVE MATERIALS UNDER

PERIODIC EXCITATIONS

by

Peng Yang

A Thesis Submitted in

Partial Fulfillment of the

Requirements for the Degree of

Master of Science

in Engineering

at

The University of Wisconsin-Milwaukee

August 2016

ABSTRACT

PHASE SENSITIVE THERMOGRAPHY OF MAGNETOSTRICTIVE MATERIALS UNDER
PERIODIC EXCITATIONS

by

Peng Yang

The University of Wisconsin-Milwaukee, 2016
Under the Supervision of Professor Rani Elhajjar and Chiu Law

The use of giant magnetostrictive materials in actuator and sensor applications is still relatively new. Giant magnetostrictive materials, such as Terfenol-D, are unique in producing large deformation under a magnetic field. Applications of these materials in solid state actuators and transducers may require more knowledge on the interaction between geometry and material properties for a specific design. In order to gain more understanding of the magnetostriction mechanism, phase sensitive or lock-in thermography has been used to study Terfenol-D. Thermography is useful in that it allows for full field measurement of the surface of an object with a relatively simple setup. By applying phase sensitive detection and lock-in amplification, small surface temperature changes caused by the magnetostriction through periodic loading can be detected. Two forms of Terfenol-D materials, monolithic and epoxy composite, are the main focus in this studied. The increase in temperature for the monolithic material is in contrast to the decrease in temperature for the composite when they undergo magnetostriction. In addition, the presence of geometric features on monolithic Terfenol D can cause variations in strain distribution. It is also observed that the detection method is quite sensitive to perturbations in strain induced by modifications of the sample geometry.

TABLE OF CONTENTS

LIST OF FIGURES

LIST OF TABLES

ACKNOWLEDGMENTS

I would like to take this opportunity to thank my two advisors, Dr. Rani Elhajjar and Dr. Chiu Law for their supervision on this research. This work could not have been done if it was not for them. I would also like to thank the University of Wisconsin-Milwaukee Research Growth Initiative for their support in this research. I would also like to acknowledge my colleagues Aleksey Yermakov and Edward Lynch for the help and advices that they have provided me over the course of this research.

I want to express my greatest gratitude and appreciation to my mentor, Dr. Rani Elhajjar, for his support and encouragement over the years. I cannot begin to describe the impact he has had in my development as an engineer. Since the first time I worked in his laboratory as an undergraduate student, he has provided a safe learning environment that allowed me to grow both professionally and personally. I attribute all my successes and experiences to him.

Lastly, I want to thank my parents, family, and loved ones for their love and support. They gave me a safe home to come to during the weekends and gave me something to look forward to at the end of a long difficult week. Their curiosity and interest in my studies has helped me stayed motivated to push my boundaries and learn new things, just so that I can share it with them.

1. INTRODUCTION

The technological growth in materials science over the last several decades has led to the development of many smart materials. In particular are giant magnetostrictive materials. These materials are magnetic materials made typically from rare earth elements. Magnetostriction is a property in which couples together both mechanical deformation and magnetic fields. Generally, all ferromagnetic materials exhibit this property; particularly, Terfenol-D has a stronger response than that of steel. Although magnetostriction in steel is very low, it is responsible for the humming noise that is heard in AC transformers.

The development of giant magnetostrictive materials has found its way into transducers, sensors, and solid state actuators. The application that most actuators fall into is in the realm of active vibration control or controlling structures. Some proposed structures are airplane wings and helicopter blades [1-3]. In addition, work has been done on utilizing these smart materials for energy harvesting by taking advantage of the Villari effect [4]. As manufacturing methods become more advance, this material can be fabricated to exploit its magnetostrictive properties.

There are several techniques that are often used for measuring and studying magnetostriction. A common direct method is strain gages although it is limited in sensitivity [5]. Another direct method is capacitance dilatometry which is capacitance displacement sensor that is more sensitive to small length changes than a strain gage. Non-direct methods include digital image correlation (DIC) and ferromagnetic resonance [6, 7]. A potential non direct technology to include is thermography.

Although the use of thermography for measuring stresses and strains is not a new idea, this technique may present a new understanding of magnetostrictive materials. Thermoelastic stress analysis is a full field thermography technique that allows the detection of stresses of a part

1

under elastic loading through infrared mapping of the surface [8]. The thermoelastic effect is the thermal response due to a physical deformation. This technique has mostly been used with metals and composites under mechanical loading. However, the use of full field thermography on magnetostrictive materials for quantifying stress and strain changes has not been previously explored in literature. The aim of this study is to investigate the thermal response of magnetostrictive materials using infrared phase sensitive thermography.

2. LITERATURE REVIEW

The use of thermal signatures for stress detection is complicated by the strict requirements on differentiating small thermal fluctuations from magnetic field induced stresses from unwanted thermal sources. The process of magnetostriction involves the interaction of many variables that can introduce heat. Some of these include eddy currents, external thermal radiation, stresses, and intrinsic properties of the magnetostrictive material. Furthermore, equipment and setup limitations can affect thermal response. In order to limit and isolate these effects, it is important that each subject matter is understood.

2.1 Magnetostriction

Magnetostriction is a property of a ferromagnetic material that deform under applied magnetic fields and becomes magnetized. This magnetostriction phenomenon was first observed in a sample of iron by James Joule in 1842 [9]. In his experiment, he found that the piece of iron had changed its length when it became magnetized. This magnetoelastic coupling can be used in sensor applications [10]. Although the presence of magnetostriction in ferromagnetic materials has been known since then, it was not until the 1970's that giant magnetostrictive materials

2

gained momentum with the development of Terfenol D. These developments lead to the creation of the two well-known giant magnetostrictive materials, Terfenol-D and Galfenol. The names of these materials are acronyms for their composition. Terfenol-D consists of terbium, iron, and dysprosium whereas Galfenol is comprised of gallium and iron. Both were developed by the Naval Ordnance Laboratory [11]. Of these two materials, Terfenol-D can achieve higher magnetostriction than Galfenol. This is due to the combination of its constituent elements Terbium and Dysprosium. The two elements allow for large magnetomechanical coupling due to the compensation of anisotropies from each individual element [12]. Terfenol-D's magnetostriction ranges from 800 to 1200 ppm which is about four times larger than that of Galfenol, which ranges from 200-300 ppm [13, 14]

The large differences in magnetostriction of these two material begs the question of why use one over the other. Galfenol, commonly fabricated with a composition of Ga_xFe_{1-x} where 0.7<x<0.22, possesses superior mechanical properties than those of Terfenol-D [15]. These properties enable it to be used in structural components while retaining its magnetostrictive properties. In addition, Galfenol can be easily machined for complex and intricate designs. Terfenol-D on the other hand is brittle which limits its applicable use and is susceptible to chipping when machining. Its tensile strength is also low compared to that of Galfenol. The added difficulty in working with Terfenol-D is that it is also pyrophoric. Although Galfenol is superior in terms of mechanical properties, the extraordinary magnetostrictive performance of Terfenol-D makes it an ideal candidate to be used for this study.

The composition of Terfenol-D is typically $Tb_xDy_{1-x}Fe_2$ where $0.27 < x < 0.3$. It has a cubic packing structure in which the growth axis of the crystal is usually in the [112] direction as shown in Figure 1. The two easy axes of magnetic domain alignment is in the [111] and [11$\bar{1}$]

3

which are 90° from each other. When a magnetic field is applied along the growth axis, the theoretical maximum magnetostriction occurs in $[11\bar{1}]$ direction [16]. In early works on experimental testing of cellular crystal, it has been found that there were no significant effect of growth direction on the saturation magnetization [17].
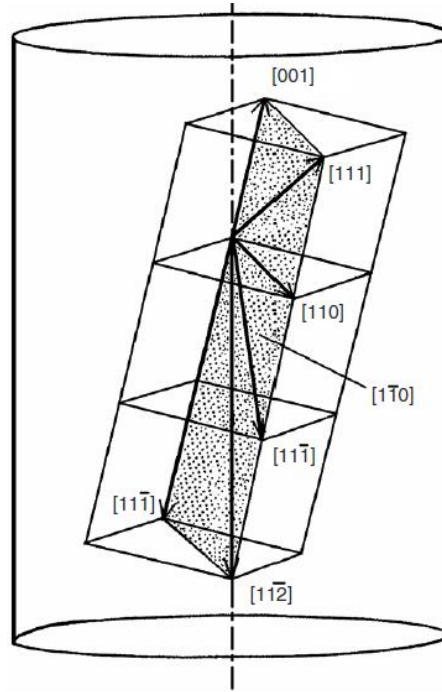
Figure 1. Crystalline Structure of Terfenol-D [18].

The root cause of magnetostriction in these materials can be traced down to the atomic scale. Here the magnetic moment of an atom is the result of its intrinsic spin moment and its extrinsic dipole moment. For rare earth metals, dipoles are more common because their anisotropically shaped electron cloud from partially filled orbital shells. The anisotropic charge distribution causes one side of the atom to be more polarized or positively charged and the other negatively charged [19]. These atoms also generate their own magnetic field since moving electron produces current which generates a magnetic field. Normally, the arrangement of these

4

moments is in such a way that the overall net magnetic field is zero. However, when an external magnetic field is applied, they align themselves with the field direction. A group of these atoms align together to form a magnetic domain. It is here that we begin to see magnetoelastic coupling. As these domains align with an increasing applied magnetic field, the overall length of the material begin to increase producing magnetostriction (Figure 2)[20]. The domains will continue to rotate as long as the applied field is increasing until they all line up. At the point when the domains are all aligned and can no longer rotate, the strain is said to be saturated.
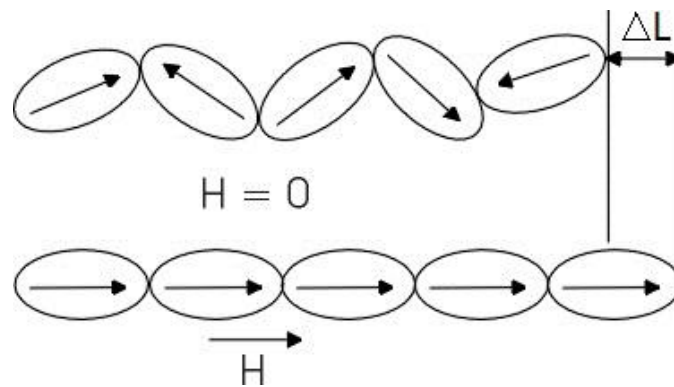
Figure 2. Change of length, ΔL, due to rotation of magnetic domains.

Magnetostrictive performance has been found to be improved when an initial stress is applied parallel to the field of magnetization before being magnetized [21, 22]. By compressing the material, the magnetic domains aligns itself towards the easy axis perpendicular to the applied field (Figure 3). As the material becomes magnetized, the magnetic domains realign thus producing a net increase in magnetostriction. In Terfenol-D, the application of a pre-stress can increase magnetostriction up to 2000 ppm [23].

5
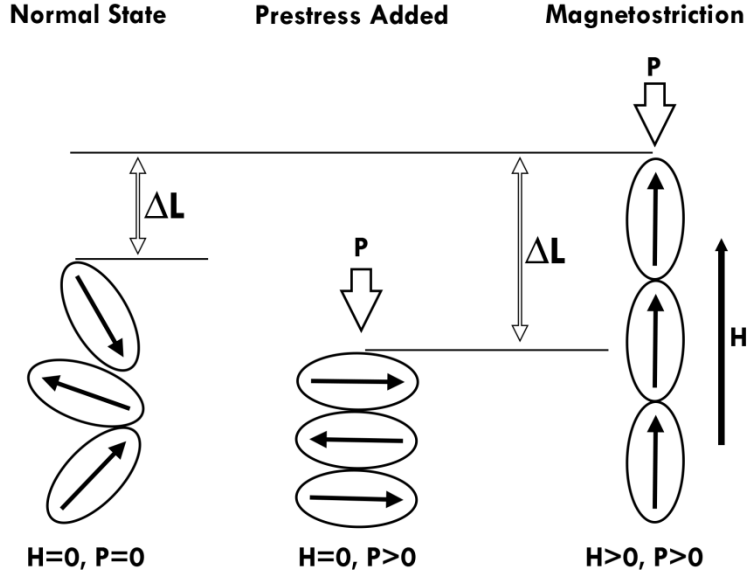
Figure 3. Effect of pre-stress on overall magnetostriction.

The energy in magnetostriction comprises of mainly magneto and mechanical work. The magnetic work, dW is a related to the change in magnetic flux density, dB, shown as [11]

$$dW_{mag} = H_m dB_m \qquad (1)$$

where subscript $m = 1,2,3$ are the coordinate axis. The mechanical work involved is related to the reversible deformation of the unit volume given as

$$dW_{mech} = \sigma_k d\varepsilon_k \qquad (2)$$

where subscript k refers to the 6 engineering strain components and σ and ε are the stress and strain, respectively. The change in total internal energy is the combination of Eq.1 and Eq.2

$$dU = \sigma_k d\varepsilon_k + H_m dB_m \qquad (3)$$

The correlation of applied field and magnetostriction can further be developed by solving the Gibbs free energy equation. For an adiabatic process this is

$$G = U - \sigma_k d\varepsilon_k - H_m dB_m \qquad (4)$$

where the change of energy is achieved through differentiating and reduces

6

$$dG = -\varepsilon_k d\sigma_k - B_m dH_m \qquad (5)$$

The partial derivative of ε_i with respect to H_m and B_m with respect to σ_i gives

$$\frac{\partial \varepsilon_k}{\partial H_m} = \frac{\partial B_m}{\partial \sigma_k} = d_{mk} \qquad (6)$$

where d_{mk} is known as the magnetostrictive or piezomagnetic constant. In actual applications, the directions of applied stress and magnetic field are generally the same thus the magnetostrictive constant is usually listed as d_{33}.

2.2 Terfenol-D Particulate Composites

The use of Terfenol-D particulates in a composite system is not uncommon and offers many advantages. Terfenol-D is a very brittle material which makes machining difficult for sensor or actuator applications. In addition, the low tensile strength limits its applicability in high stressed situations. Imbedding Terfenol-D in a polymer matrix greatly improves its strength and toughness. Another advantage that a composite has over a monolithic material is the reduction in eddy current losses. In monolithic Terfenol-D eddy current loss reduces the efficiency of the magnetostrictive response and limits the frequency range [20, 24].

There have been a number of studies in Terfenol-D composites and its magnetostriction response. It has been found that the use of polymer matrix with various the volume percentages of Terfenol-D can change the magnetostriction of the material [25, 26]. A lower volume fraction of Terfenol-D particles will improve operation at higher frequencies while reducing eddy current loss. Particle alignment in a magnetic field during fabrication has also shown to improve magnetostriction compared to one with randomly aligned particles [27]. This anisotropic behavior opens doors for customization of sensors and actuators.

7

Another benefit of using a Terfenol-D as a composite is the stresses that are introduced to the particles. Depending on the type of binder, it can introduce residual stresses once cured due to the binder shrinking. Depending on the application, this can be a positive effect. Residual stress from the shrinking matrix has shown to generate a pre-stress on the particles which assists with magnetization [28].

2.3 Magnetocaloric Effect

In addition to magnetoelastic coupling there is also magnetocaloric coupling. The magnetocaloric effect (MCE) is the thermal response in a magnetic material when subjected to a change in magnetic field. The first known documentation of this effect was by Warburg in 1881 [29]. In his early observations he saw temperature changes in a piece of iron when adding and removing it from a magnetic field. The cause of MCE is related to the internal energy of the material system. The entropy associated with this system is a combination of both the magnetic ordering of domains and the temperature of the system [30]. In a material system, the magnetic moments are generally randomly orientated. This disorientation is due to thermal energy that was inputted into the system, increasing energy state, which agitated the moments during the formation of the material. When a magnetic field is applied under adiabatic conditions, the magnetic moments rotate to the direction of magnetization which is a lower energy state. The result is heat being released to compensate for the rotation since the total entropy remains the same [31]. The opposite effect occurs when the magnetic field is removed. The magnetic moments return to their original position absorbing thermal energy in the process (Figure 4).

8
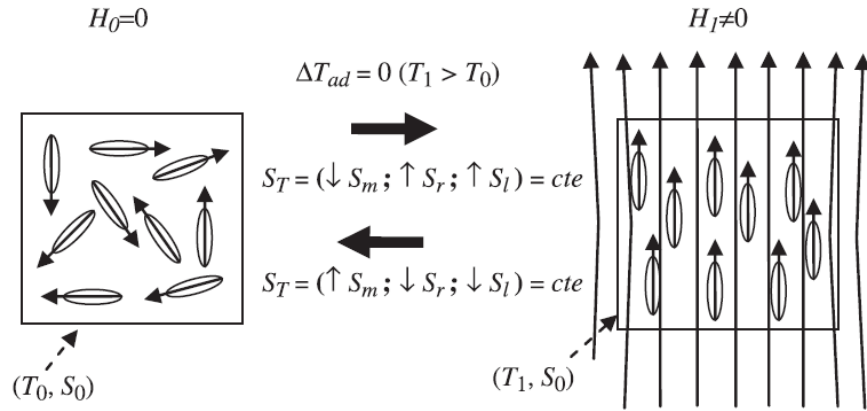
Figure 4. Magnetocaloric effect caused by rotation of magnetic domains releasing heat during the process [31].

MCE can be found in ferromagnetic and paramagnetic materials. However, MCE exhibits the greatest response in rare earth alloys. This is due to their high molecular weight and magnetic structures. Magnetocaloric materials are usually categorized into two groups. Materials that experiences MCE are considered to be magnetocaloric materials but the ones that experiences this effect to a large degree are considered to be giant magnetocaloric (GMC) materials. Terfenol-D has been known to experience MCE to a degree but it is not typically considered a GMC material such as $Gd_5Si_{1.8}Ge_{2.2}$, which is classified as both a GMC and colossal magnetostrictive material. The MCE that $Gd_5Si_{1.8}Ge_{2.2}$ exhibits can range from 0 to 18K [32]. The differences in these two materials are that the magnetostriction in Terfenol-D is gradual with increasing field whereas $Gd_5Si_{1.8}Ge_{2.2}$ experiences sudden magnetostriction after the magnetic field reaches a "threshold" [33].

The measurement of the MCE is done by either direct or indirect methods. Direct methods include thermocouples, thermal cameras, and contact measurements in which the temperature change can be directly measured. Indirect utilizes theoretical formulations based on relations from other properties. In direct methods, an initial temperature measurement is taken with no magnetic field applied. Then, a magnetic is applied quickly to achieve adiabaticity and

9

the temperature change is recorded. Special test setups are generally required in order to achieve adiabatic conditions including thermally insulated chambers and near vacuum operation [30].

The general theoretical thermodynamic formulation for MCE is related to the internal energy of the system which is a combination of the magnetic work, volume, and temperature can be expressed as [31]

$$dU = TdS - pdV - HdM \tag{7}$$

Where T is the temperature, S is the entropy, p is the pressure, and V is the volume. In a system with no volume change where $dV = 0$ the internal energy is simplified to

$$dU = TdS - HdM \tag{8}$$

The temperature change from magnetization can be determined by the total change in entropy. This can be written as

$$dS = \left(\frac{\partial S}{\partial T}\right)_H dT + \left(\frac{\partial S}{\partial H}\right)_T dH \tag{9}$$

The partial derivative of entropy with respect to temperature is equivalent to the heat capacity and the partial derivative of the entropy with respect to the magnetic strength is equivalent to the partial derivative of magnetization with respect to temperature:

$$\left(\frac{\partial S}{\partial T}\right)_H = C_H \tag{10}$$

$$\left(\frac{\partial S}{\partial H}\right)_T = \left(\frac{\partial M}{\partial T}\right)_H \tag{11}$$

In an adiabatic system, $dS = 0$ and substituting Eq.10 and Eq.11 into Eq.9 yields the change of temperature for MCE

10

$$dT = -\frac{T}{C_H}\left(\frac{\partial M}{\partial T}\right)_H dH \qquad (12)$$

2.4 Phase Sensitive Lock-In Thermography

The use of infrared radiation for quantitative and qualitative measurement is known as thermography. Modern day thermography consists of using an infrared camera for full field inspection. Thermography methods are generally divided into two categories, steady state and dynamic. Steady state thermography is used for measuring large temperature ranges such as monitoring heat transfer in pipes or insulations where the temperature remains relatively constant. For detection of small temperature ranges, dynamic or active thermography is usually preferred. The benefit that dynamic thermography has over steady state thermography is that it is able to detect transient and small changes in temperature caused by presence of certain elements inside a material such as defects and damages. It does this by taking advantage of the differences in the heat transfer rate. Under this method, several techniques exists such as pulse thermography (PT) and lock-in thermography (LT) [34]. The subcategories for PT are flash and transient while the subcategories for LT is phase sensitive and periodic heating as shown in Figure 5.

11
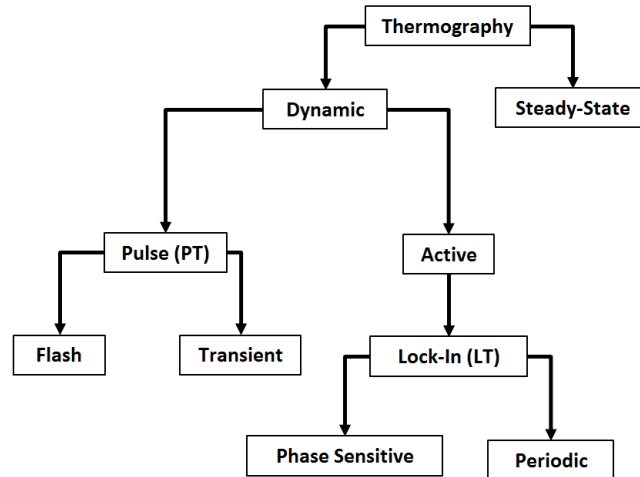
Figure 5. Hierarchy of thermography

The concept behind PT is to use infrared radiation emitted from the material to inspect it. A material with an internal void or crack, for example, will have higher heat conduction rate in the area around the defect, which will affect the emitted radiation. The difference in conduction rate produces a surface temperature gradient that is captured by the infrared camera. The main difference between flash and transient thermography is that flash is usually used to inspect small areas relatively quickly and transient is used to inspect larger area which takes much longer. Flash thermography uses short burst of high energy light source such as a xenon lamp that is directed to the surface of interest revealing shallow defects. For the transient method, a low heat source is applied for the detection of deeper defects [35, 36]. The limitation for PT is that the temperature range must be higher than that of the noise level in the camera. Otherwise the camera detector cannot distinguish these thermal signatures from noise. This limits the temperature range that PT can be used [37].

The problem of measuring small temperature changes, usually under 100mK, is the noise equivalent temperature difference (NETD) in an infrared camera. NETD is the noise introduced from outside sources, such as electronics, the environment, and even the camera itself which is

12

equivalent to a temperature range of the targeted area [38]. For example, if an actual signal produced is a step function shown in Figure 6(a) and the NETD signal is shown in Figure 6(b), which is much larger than the step function, then captured information will be displayed as in Figure 6(c). The signal of interest is too small and is buried by the noise. A solution to uncover the signal is to use lock-in thermography with signal modulation such as phase sensitive detection. This gives infrared cameras the ability to detect tiny temperature changes down to 5mK (and in some cases even lower), where the NETD of sophisticated infrared camera is around 20mK and 50mK [39].
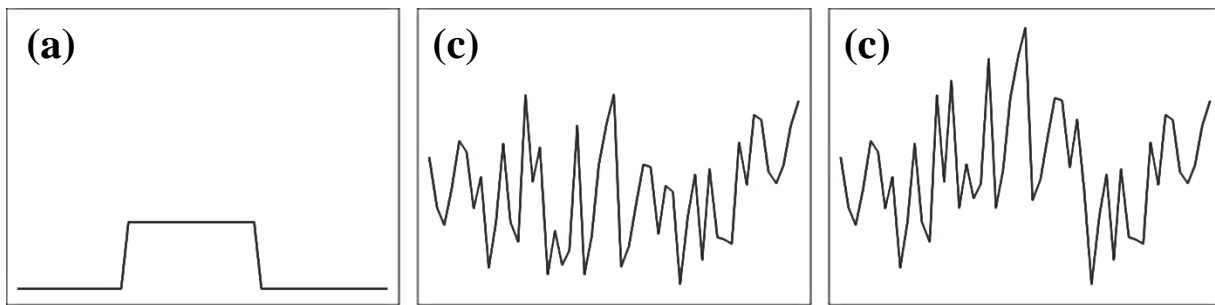
Figure 6. (a) Actual step signal. (b) Noise in the camera. (c) Captured signal with the presence of noise.

LT revolves around the principle of averaging an AC signal through periodic pulsing or modulation over time to suppress the noise. It can be achieved by feeding a lock-in signal processing system with the captured signal and a reference signal. The reference signal can be generated internally or taken directly from the source when the test is performed. These two signals are passed onto a correlating procedure as shown in Figure 7. First, the signal input is passed through a filter to initially remove any noise associated with it and the reference signal is passed through a phase shifter to synchronize the two signals. Next the two signals enter a mixer where they are multiplied together which produces a 'demodulator output'. The demodulated

13

output signal is then integrated and averaged over a set period. The averaging reduces any noise that has passed through the filter.
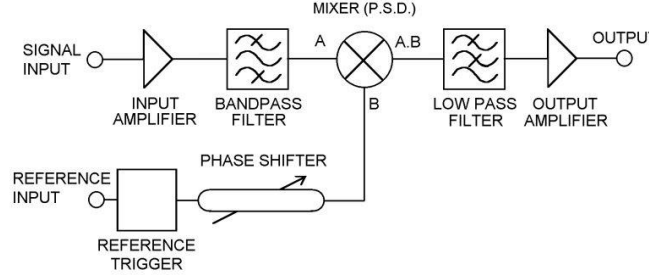
Figure 7. Schematic showing correlating procedure [40].

This process can be described mathematically through one-channel correlation. Given an input signal $F(t)$, which contains noise, and its weighing factors based on the reference signal, $K(t)$, the demodulated DC output is calculated as [37]

$$S = \frac{1}{t_{int}} \int_0^{t_{int}} F(t)K(t)\, dt \tag{13}$$

where t_{int} is the averaging time. This is further illustrated in Figure 8. The sinusoidal captured signal, $F(t)$, has a signal with an amplitude of 0.1 imbedded in a random noise with the variation at a level of 0.9. Clearly the noise has covered up the signal of interest which is indistinguishable from the noise. Next we have a noise free reference signal, $K(t)$, with which we can 'demodulate' the noisy signal by multiplying it with $F(t)$. For simplicity, the input and reference AC signal are assumed to be in-phase with each other. By averaging and integrating the demodulated signal over a set period, we can see that the DC output converges to a single value of 0.1 which is the amplitude of the signal. The advantage of LT is that over many cycles of averaging, the DC resolution increases and the noise level is suppressed.

14
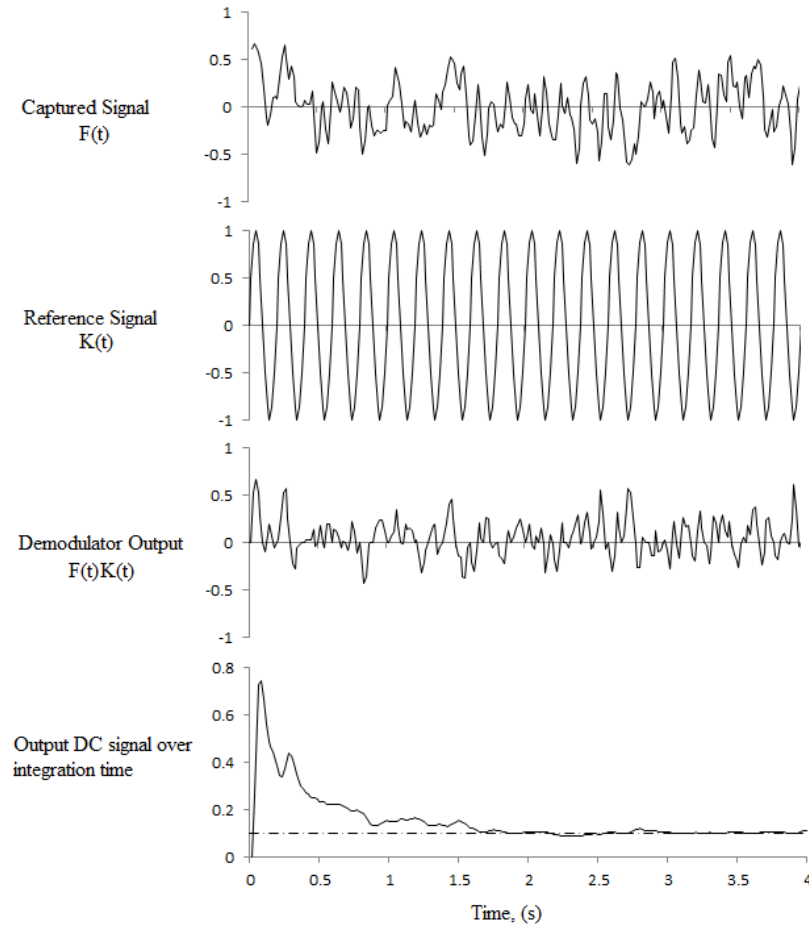
Figure 8. Signal processing using the correlation procedure.

2.5 Thermoelastic Stress Analysis

Lock-in or phase-sensitive thermography has been applied to nondestructive evaluation of electronics and aerospace composite materials [41-43]. It has found its way into full field stress measurement. Thermoelastic stress analysis (TSA) is an experimental technique that relates the change in temperature in response to a change in elastic strain. This allows the interrogation of structures to reveal areas of high stress concentration or the distribution of stress with confirmations from numerical simulations. It can also be used to find damage initiation and progression in parts [44].

15

The TSA method requires a component that is cyclically loaded. An infrared camera is used to monitor the change in temperature with the addition of a reference signal. The reference signal is obtained either through measurement from a strain gage or the load cell signal. The temperature change from thermoelastic stress measurement is usually very small in the order of milliKelvins thus a lock-in amplifier is required.

The general internal energy equation for thermodynamics of thermoelastic stress is written as

$$dU = \sigma_{ij}d\varepsilon_{ij} + SdT \quad (i,j = 1,2,3). \tag{14}$$

By applying the second law of thermodynamics along with state functions describing the state of the system, the change in entropy of the system this is described as (see references [45] and [46] for in-depth derivation)

$$dS = -\frac{1}{\rho}\frac{\partial \sigma_{ij}}{\partial T}d\varepsilon_{ij} + c_\varepsilon \frac{dT}{T} \tag{15}$$

Under adiabatic conditions where $dS = 0$ and applying Lamé elastic parameters which are assumed to be independent of temperature, we arrive at the classical theory of thermoelastic stress [46]:

$$\Delta T = -K_m T_o \Delta(\sigma_1 + \sigma_2) \tag{16}$$

$$K_m = \frac{\alpha}{\rho c_p}$$

where K_m is the thermoelastic constant that is equivalent to the coefficient of thermal expansion divided by the material density, ρ, and specific heat capacity at constant pressure, c_p. T_o is the initial temperature, and σ_1 and σ_2 are the first and second principle stresses, respectively. From equation (16), a positive or tensile stress will cause the sample temperature to decrease and a negative or compressive stress will cause the sample temperature to increase.

16

The temperature change associated with the loaded sample is achieved through adiabatic heating. In practice, under certain loading frequencies, usually 3-10Hz, the sample will exhibit adiabatic-like conditions were there temperature change in the part remains relatively constant. If the frequency is above these values the thermal signal begins to become attenuated due to thermal drag down in metals [47]. In polymers, the higher frequency is preferred due to viscoelastic heating. Under non-adiabatic condition, heat is lost through both convection and conduction. Unless the convection rate is high, the primary mechanism is conduction of heat inside the material. This can lead to an underestimation of stresses involved [48].

Infrared detection is accomplished by painting the sample matte black. This allows the sample to mimic a black body by increasing its thermal emissivity. The sample layer applied needs to be thin enough to cover the sample uniformly but not too thick to cause insulation. A coat of thick paint becomes a 'witness' layer, where the thermoelastic effect seen is associated with the paint coating and not the base material [49].

3. EXPERIMENTAL SETUP

3.1 Fabrication of Specimens

Eight test samples were used in this study. They are two monolithic Terfenol-D samples (larger and smaller), aluminum, three Terfenol-D/epoxy composites, a ferrite/epoxy composite, and a pure epoxy. In order to make sure that the thermal response was a result of magnetostriction and not from other sources, several samples were used as controls to isolate this effect. The control samples in this test were the pure epoxy, aluminum, and ferrite/epoxy composite. Pure epoxy was used in order to ensure that no other sources of thermal emissions were present except those from thermoelastic effects. Aluminum which has a low permeability

17

was used to determine if eddy current loss are present with the applied AC magnetic field in the monolithic sample. Ferrite which has a relative permeability similar to Terfenol-D [50] was used in the ferrite/epoxy composite to determine if any other thermal effects were present in the Terfenol-D/epoxy samples, either through magnetic effects such as eddy current loss or thermoelastic effects due to particle attraction.

Table 1. Table showing the control samples and the variables they are to isolate

Control	Sample to be Compared With	Control Variables	
		Thermoelastic Effect from Setup	Eddy Current Loss
Epoxy	Monolithic and Composite	X	
Aluminum	Monolithic		X
Ferrite/Epoxy	Composite		X

The Terfenol-D that was used in the experiment was obtained from Etrema with its properties shown in Table 2 [14]. The samples used are shown in Table 3 along with their ID. The monolithic samples were a rectangular bar with sample TML having a nominal dimension of $6.36 \times 6.36 \times 36.2$ mm $(0.25 \times 0.25 \times 1.43$ inches) while the smaller sample, TMS, had a nominal dimension of $5 \times 5 \times 24$ mm $(0.2 \times 0.2 \times 0.94$ inches). The Terfenol-D/epoxy and ferrite/epoxy (FE) were fabricated with Terfenol-D and ferrite particles, respectively. The particulate sizes ranged from 150 to 350 μm and was mixed with epoxy (SuperSap 100/1000, Entropy Resins, Hayward, CA) (see Table 4). The particle mixed epoxy was then placed inside a silicon mold to cure for 24 hours. After curing, the samples were grinded to their final dimensions of $5.78 \times 4.27 \times 29.64$ mm $(0.23 \times 0.17 \times 1.17$ inches) and have a weight fraction from 0.86 to 0.87 that corresponds to a volume fraction of around 0.44 to 0.46, respectively. The three Terfenol-D/epoxy samples that were produced from this process contained particles that were aligned randomly (TER), 0° (TE0) or along the long axis, and 90°(TE90) or perpendicular

18

to long axis. The alignment process for orientating particles to their designated direction was performed by placing the epoxy mixture between two neodymium rare earth magnets while it was still wet. The magnets were separated at a distance of 10.8 cm (4.25 inches) resulting in a magnetic field of 485 Gauss. When the epoxy was semi-cured in its tacky-thick gel state, the magnets were removed to allow the particles to relax from any magnetostriction introduced by the magnets. A pure epoxy and aluminum sample with the same dimensions were also fabricated.

Table 2. Physical properties of Terfenol-D

Terfenol D Physical Properties		
Mechanical Properties		
Density	9200	kg/m^3
Bulk Modulus	90	GPa
Tensile Strength	28-40	MPa
Compressive Strength	300-880	MPa
Thermal Properties		
CTE	11	Ppm/^{o}C @ 25°C
Specific Heat	330	J/(kg-K)
Magnetostrictive Properties		
Strain	800-1200	ppm
Piezomagnetic Constant	6-10	nm/A
Magnetic Properties		
Relative Permeability	2-10	

19

Table 3. Sample dimensions.

Sample ID	Description	Length, mm (in.)	Width, mm (in.)	Thickness, mm (in.)	Mass, g (oz.)	Density, kg/m^3 (lb/ft^3)	Particle wt. Fraction
EP	Epoxy	29.63 (1.167)	6.06 (0.239)	4.25 (0.167)	0.846 (0.030)	1103 (68.91)	-
FE	Ferrite/Epoxy	29.72 (1.169)	5.86 (0.230)	4.31 (0.169)	1.894 (0.067)	2519 (157.2)	72%
TER	Terfenol-D/ Epoxy (Random)	29.58 (1.163)	5.78 (0.227)	4.20 (0.135)	2.919 (0.103)	4065 (253.8)	83%
TE0	Terfenol-D/ Epoxy (0°)	29.67 (1.167)	5.73 (0.225)	4.32 (0.170)	3.377 (0.119)	4585 (286.2)	87%
TE90	Terfenol-D/ Epoxy(90°)	25.68 (1.010)	5.84 (0.230)	4.25 (0.167)	3.478 (0.123)	4680 (292.2)	87%
AL	Aluminum	29.54 (1.162)	5.08 (0.200)	5.05 (0.199)	1.995 (0.070)	2638 (164.7)	-
TML	Lg. Monolithic Terfenol-D	36.20 (1.424)	6.04 (0.238)	6.12 (0.241)	12.500 (0.441)	9341 (583.1)	-
TMS	Sm. Monolithic Terfenol-D	23.68 (0.931)	5.00 (0.197)	4.98 (0.196)	5.404 (0.191)	9165 (572.2)	-

0.5mm
(0.05mm DIV)
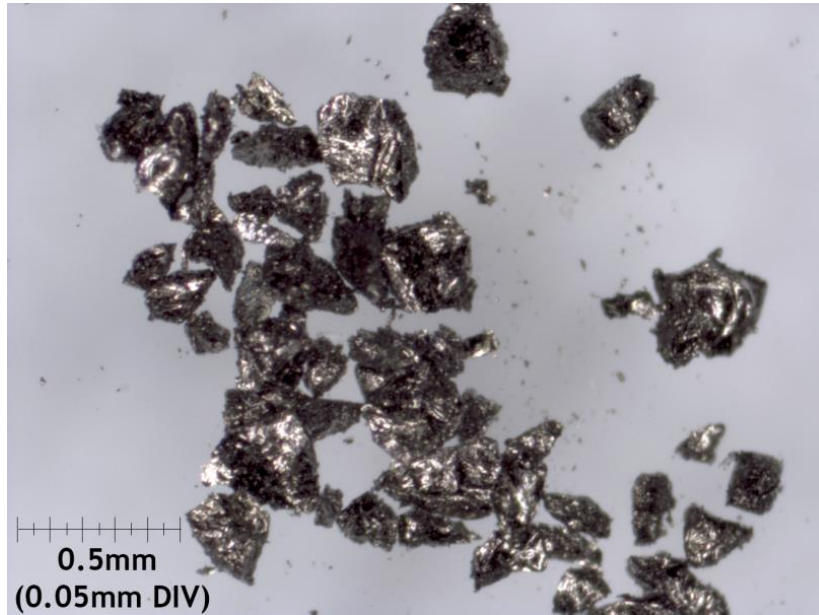
Figure 9. Terfenol-D particles under a microscope showing granular structure.

20

Table 4. Properties of SuperSap 100/1000.

SuperSap 100/1000 Properties		
Density	1100	kg/m^3
Tensile Modulus	2.62	GPa
Tensile Strength	56	MPa
Compressive Strength	72	MPa

After curing, the surface of the composites were grounded and micrographs were taken as shown in Figure 10. From these images we see that particle alignment is present in both TE0 and TE90 samples. In addition, compared to TER and FE, particle distribution is not completely uniform. The aligned particles tend to form long columns and chains extending towards the direction of the applied field during the curing process creating resin rich areas.

5mm

Figure 10. Microstructure of particulate composite samples. (From top to bottom) FE, TER, TE0, and TE90.

21

3.2 Thermo-Magneto-Mechanical Test Setup

A large electromagnet driven by an AE Techron 7224 power amplifier paired with an Agilent 33120A waveform generator was used to create a relatively uniform magnetic field between the gap of the electromagnets for measurements (Figure 11 ①, ②, and ③). The mag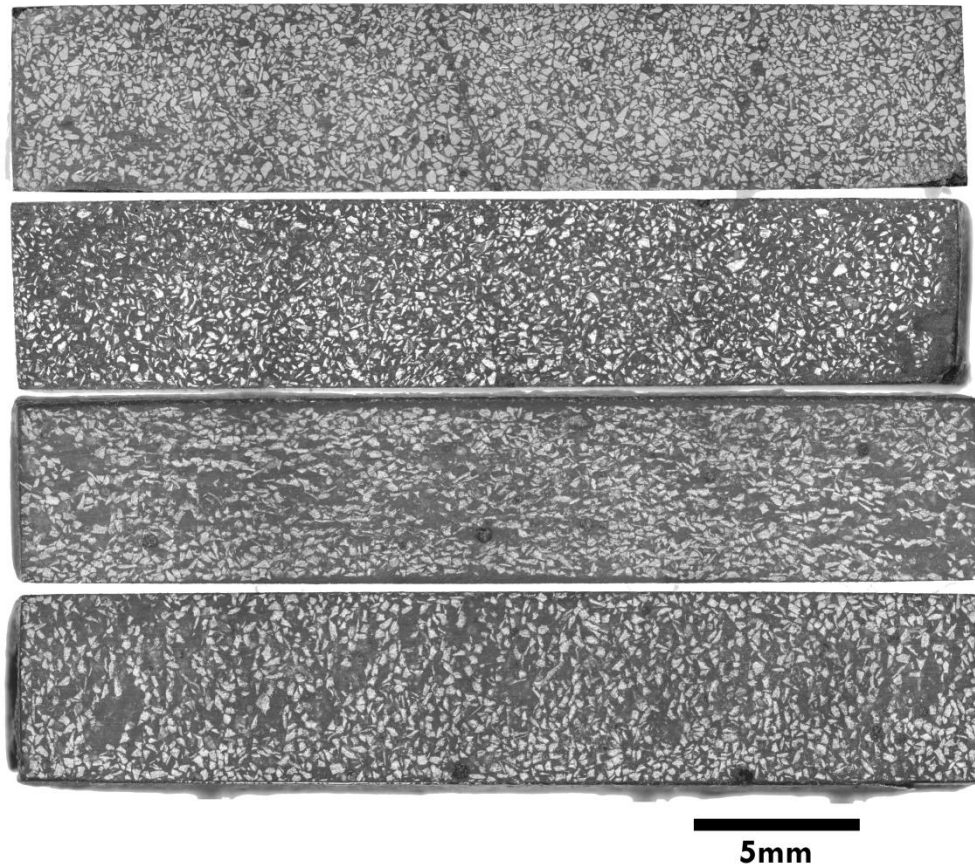netic field, B, was measured using a Sypris Model 5180 Gauss/Tesla meter, ⑥. The hall probe faced the longitudinal direction and was positioned at the middle of the specimen's long surface ⑤. According to the tangential boundary conditions for the magnetic field, the magnetic field intensity inside the specimen can be inferred by the magnetic field intensity $H = B/\mu_o$ parallel to the surface outside the specimen where B is the measured magnetic flux density value and μ_o is the permeability of free space [7].

A non-magnetic clamp was important for holding the specimen with a constant force. It also needed to be compact enough to be able to fit between two magnetic poles without disturbing the magnetic field. In both the strain gage and thermography test, a custom clamp made of ABS was 3D printed (Figure 13). The clamp has low profile and uses a single ply of plain weave carbon fiber epoxy composite as a leaf spring. The extreme bend in the spring allowed for a region of relatively constant applied force in its load-deflection profile, which cannot be achieved easily with metallic springs under the same constraint. The low profile clamp allows for the two magnetic poles to be positioned close to form a narrower gap which is important for achieving high magnetic fields. The sample was held in place with the clamp by applying a force of about 4.5N (1 lbf). This was sufficient for preventing the sample from moving while allowing the sample to strain freely. The force applied produced a negligible effect with pre-stress of less than 170 kPa (24.7 Psi). The clamp was attached to a 12.7 mm (0.5 inch) diameter solid aluminum rod that was wedged between the two magnetic poles creating a 56 mm

22

(2.20 inch) gap as shown in Figure 12. The aluminum rod allowed the positioning of the sample between the two cores.

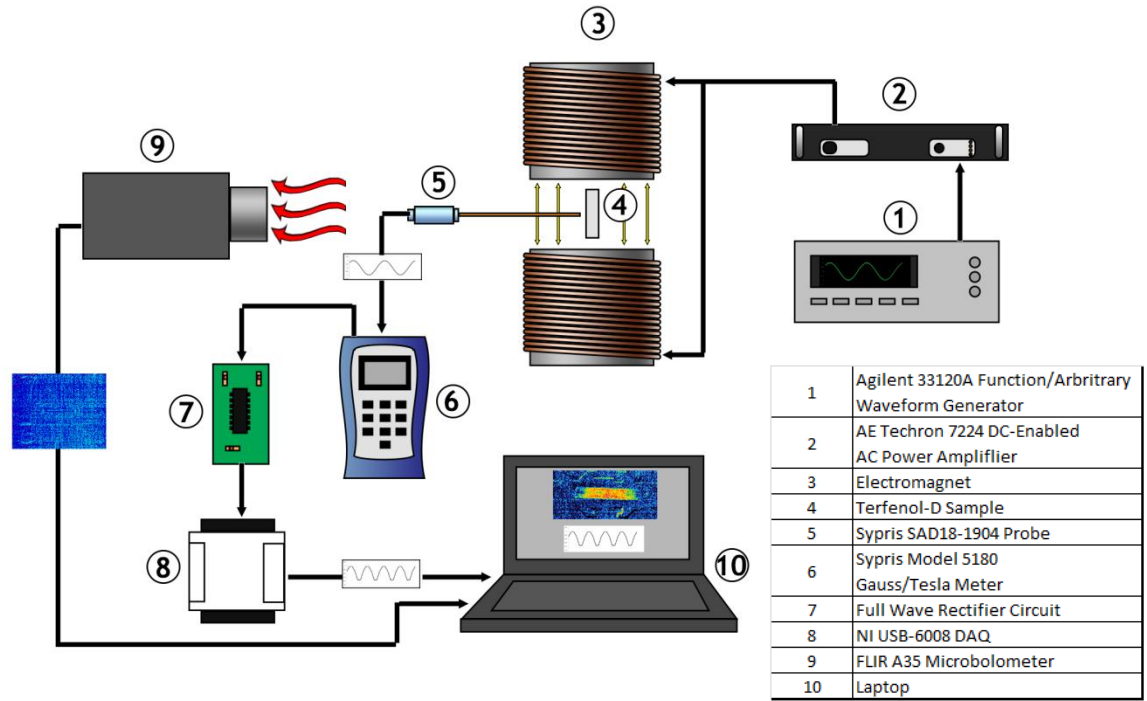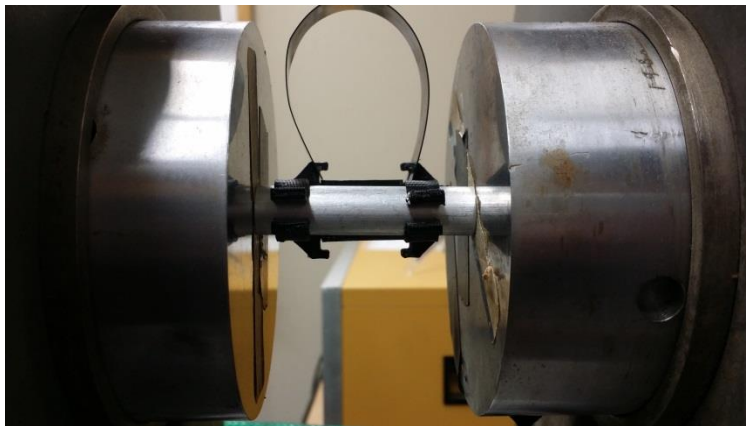|	
1	Agilent 33120A Function/Arbritrary Waveform Generator
2	AE Techron 7224 DC-Enabled AC Power Ampliflier
3	Electromagnet
4	Terfenol-D Sample
5	Sypris SAD18-1904 Probe
6	Sypris Model 5180 Gauss/Tesla Meter
7	Full Wave Rectifier Circuit
8	NI USB-6008 DAQ
9	FLIR A35 Microbolometer
10	Laptop

Figure 11. Setup of thermography evaluation on magnetostriction.

Figure 12. Aluminum rod is used as a wedge between two magnetic cores that allows the ABS clamp to be manually positioned.

23

www.manaraa.com

3.3 Strain Gage

Strain measurements were obtained from an Omega Precision strain gage mounted on the TML sample. The strain gage has a resistance of 350 ohms with gage factor of 2.13 and a dimension of 4×3 mm. The strain gage was mounted according to the manufacturer's procedure with the gage attached to the clean surface of the Terfenol-D with adhesive glue. The lead wires from the gage were tapped to the sample in order to prevent them from breaking or introducing noise from the wire movement. The sample was then placed inside the 3D printed clamp as shown in Figure 13.
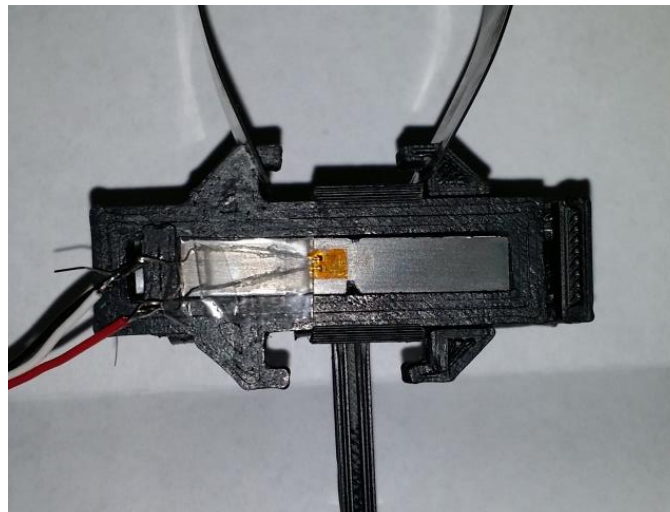
Figure 13. Terfenol-D sample mounted with strain
gage in 3D printed clamp.

The strain measurement was performed by driving the electromagnet with a 0.1Hz sinusoidal AC current that generated a magnetic field varying from -1200 to +1200 gauss. The low frequency was used to ensure that no current was induced into the lead wires by the changing magnetic field. Data points were collected with LabVIEW's NI 9236 at a sampling rate of 1000 Hz.

24

3.4 Digital Image Correlation

DIC was performed on sample TML using two 5 megapixel couple charged cameras (CCD) with 50 mm Xenoplan lens. This allowed for the zooming in and out of sample surface. The captured images were then processed using a 3D Digital Image Correlation setup (Q400; Dantec Dynamics, Germany) which applied the correlation algorithm to track pixel displacements.

The surface of the Terfenol-D was painted white to create a uniform colored surface. For tracking the displacement by the camera, a mist of black paint was then sprayed on with very close attention paid to the distribution and size of the droplets to generate a speckled pattern. Then two notches were engraved at the center of the TML sample for a clamp to hold it in place. This allowed the two ends to freely expand when the magnetic field was applied (Figure 14). The sample and the clamp were placed between two magnets where an initial reference image was taken without applied field. The second image was taken under a magnetic field of 149 kA/m.
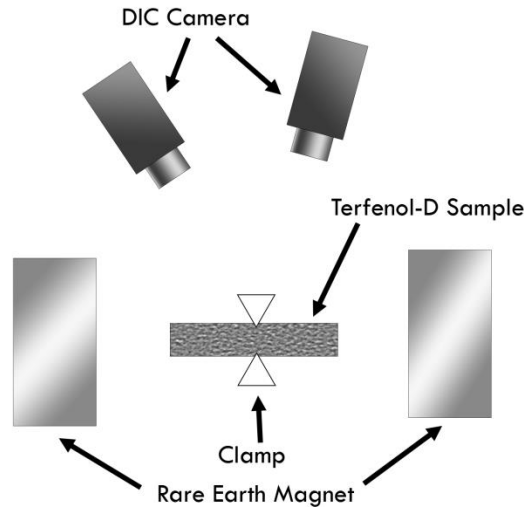
Figure 14. (Top) Terfenol-D rectangular bar showing speckled surface and notch where it was clamped for DIC. (Above) Setup for DIC

3.5 Phase Sensitive Thermography

The setup for phase sensitive thermography is shown in Figure 11. A FLIR A35 microbolometer camera, ⑨, was mounted facing towards the Terfenol-D, ④, sample between the electromagnets. The camera has a resolution of 320x256 pixels and a frame rate of 60 Hz. The NETD of the camera is 50mK. This value is high but has been shown to have little effect in thermal readings with signal processing and processing time [51, 52]. The microbolometer was connected to a computer, ⑩, running the Microbolometer Thermoelastic Evaluation (MiTE) software [53]. In addition, a NI-6008 data acquisition device was connected and served to be the reference signal input for the software Figure 11⑧.

The reference signal for the analysis software was the analog output of the gauss meter which outputs a ± 3 volts corresponding to ± 3000 Gauss. This analog signal was fed through a

26

full wave rectifier, ⑦, to convert the output into a unipolar signal with a peak value of +3 volts before reading by the NI USB-6008. The reason for the rectification was that the magnetostriction is independent of the polarity of the AC field. As a result, the magnetostriction occurs at twice of the field frequency for a sinusoidal field with zero offset [14]. The AC magnetic field was set to run at 2.5 Hz which is equivalent to a 5Hz magnetostriction of the Terfenol-D. Six amplitudes of increasing field intensity ranging from 32 to 91 kA/m were used to investigate the change in temperature for the TML and TMS sample. Samples TER, TE0 and TE90 used single amplitude of 98 kA/m, which was the maximum attainable field owing to the limitation of the setup. The MiTE program was set to average over 20 cycles of measurements to obtain one block of data. 50 blocks of data was recorded and averaged to obtain the final result.

The sample was spray painted black using Krylon Ultra Flat Black paint to increase the emissivity of the material. This paint has been shown to have an emissivity of 0.94 [54]. The paint layer was measured to be approximately 10 microns thick, which was an ideal thickness for this study. To verify this, three different thickness of 10, 20, and 30 microns of paint were applied to the monolithic Terfenol-D. Previous research have shown that the thickness of the paint layer can affect both the attenuation and lagging in the temperature response [55]. The effects of interest were the change in temperature with respect to the applied magnetic field (dT versus H).

4. FINITE ELEMENT MODELING

In addition to the experimental testing, a finite element model was created to correlate results using ANSYS Mechanical APDL version 16.2. Only the monolithic Terfenol-D samples were simulated. Quarter models of both TMS and TML samples were constructed with a mesh of

27

20 node brick elements with two planes of symmetry as shown in Figure 15. The dimensions are equivalent to the actual test sample. One of the key geometrical aspects of the model on the left in Figure 15 is the notch, which was present in the TML sample. The notch was modeled as a semicircle with a radius of 0.5 mm (0.02 inch)

Magnetostriction was simulated through using a thermal expansion analogy where the coefficient of thermal expansion in the program was redefined as the piezomagnetic constant, d, and applied temperature was redefined as the applied magnetic field. It has been found in literature that under magnetostriction, the transverse strain is about half of the axial strain [7]. For the model, the coefficient of thermal expansion (CTE) in the X-direction was set as d and the CTE in the Y and Z directions were set as $-0.5d$ to simulate this effect. In order to examine the strain field in the part, a thin face is created to act as a 'witness' surface. This is so that the program can register stresses and strains. The property of this surface is the same as the bulk volume but with no temperature applied.

The boundary conditions were set to be similar to that of the actual test setup. The symmetrical planes allow the elements to deform freely in-plane (X and Y planes) while preventing it from displacing out of plane. The back surface was constrained to prevent displacement out of plane (Z-direction) but allow for deformation in-plane. The pre-stress was not included in the finite element model.
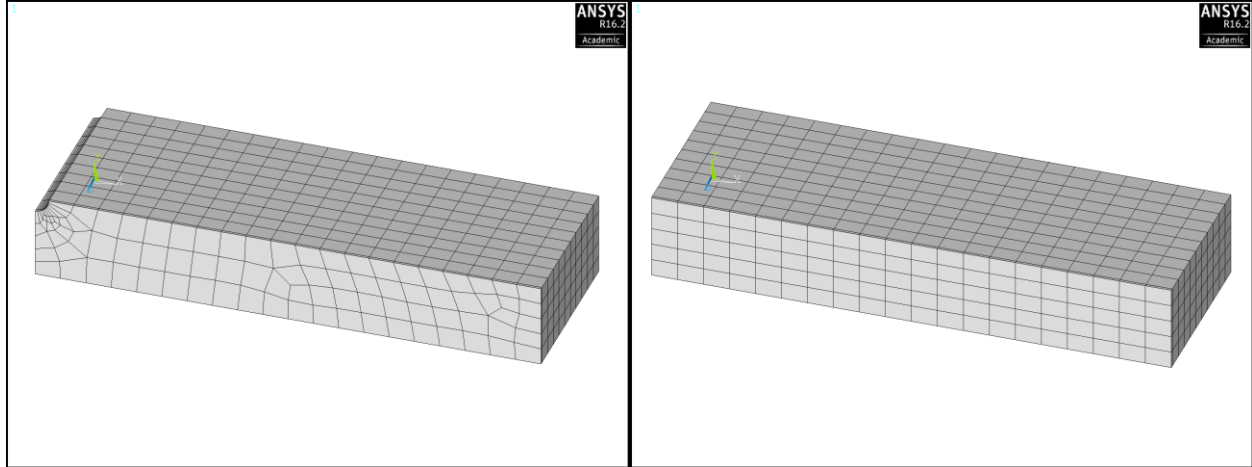
Figure 15. ANSYS 1/4th model of monolithic Terfenol D. (Left) Model with a notch representing TML. (Right) Model without notch representing TMS.

5. MONOLITHIC TERFENOL-D RESULTS

Results from the magnetic cycling revealed temperature changes for the monolithic Terfenol-D sample and Terfenol-D/epoxy samples with 0°, and 90° alignment. The sample was held in place by using a clamp applying 4.5N of force. The samples were also allowed to strain during magnetostriction. Temperature response was absent in the epoxy, aluminum, and ferrite/epoxy samples verifying that other sources of heat, either from eddy currents or external stress, were not present.

5.1 Phase Sensitive Thermography Results

Results from periodic magnetic field excitation revealed temperature changes for the monolithic Terfenol-D (see Figure 16 and Figure 17. The left image in Figure 16 is a depiction of the microbolometer's point of view of the whole setup and the right set of images focuses on the response of TML. The temperature changes seen in the sample ranges from 0 to 15mK. There were several features captured by Figure 16. First, the temperature change became greater as the magnetic field was increased. Second, the change in temperature was not uniform throughout the

29

sample. The greatest change occurred towards the center and the least change was at the two ends. Third, the temperature change was greatest along the top and bottom edge while the center portion experienced lesser amount. Lastly, there were certain distinct features that were consistently present in each image.

In Figure 17, similar trend of temperature changes was observed in the TMS sample with respect to the applied magnetic field. A vertical discontinuity region of low temperature change was seen towards the right edge. The top edge seemed to experience a higher change in temperature compared to the bottom edge. The horizontal distribution of the temperature did show more uniformity than the large sample in Figure 16.
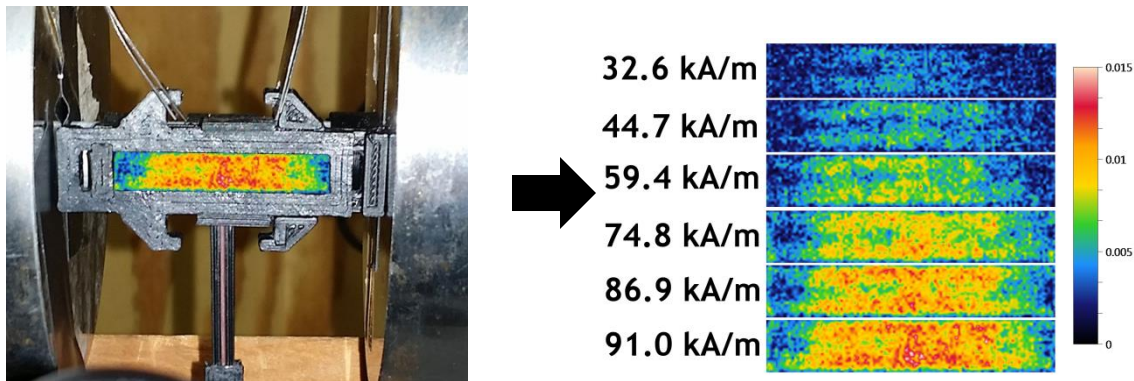

Figure 16. (Left) Image of sample depicting microbolometer's point of view. (Right) Thermal images of change of temperature for TML sample in response to applied magnetic field at varying field strength. Temperature scale is in Kelvins.
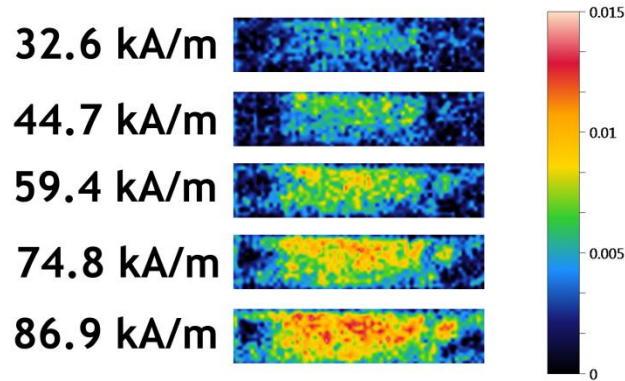
Figure 17. Change in temperature versus applied magnetic field for the TMS sample.
Temperature scale is in Kelvins.

The effect of paint layer thickness is shown in Figure 18 for the TML sample. From this image, it is apparent that the temperature change was not affected by the thickness of paint. However, the distinct thermal gradient regions in these images seemed to be clearer as paint layer thickness increased.
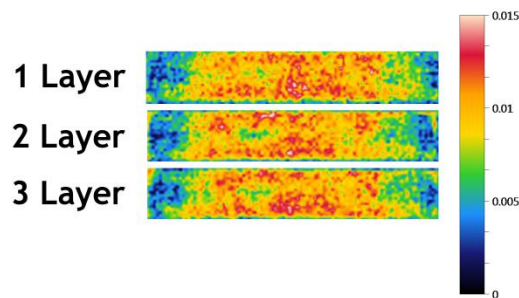
Figure 18. Effect of paint layer thickness. Each paint layer thickness is approximately 10 microns thick.

These regions on the Terfenol-D were investigated further by carefully removing the paint layers without damaging the Terfenol-D's surface and reapplying it. If these regions were a result of the paint layer, then they would disappear when the layer was reapplied and the test was repeated. Otherwise, if they were to still exists, then these regions maybe the result of the

material variability or geometrical effects. Upon removing the paint layer, no visual microstructural effects were seen.

The temperature data at various magnetic field values H from Figure 16 were plotted on a graph in terms of their average temperature and the applied magnetic field in Figure 19. The temperature was taken as averages over the sample excluding the ends since the change at the ends were much lower compared to the center area. From this we see that the temperature change is linear. As the field increases so did the change in temperature.
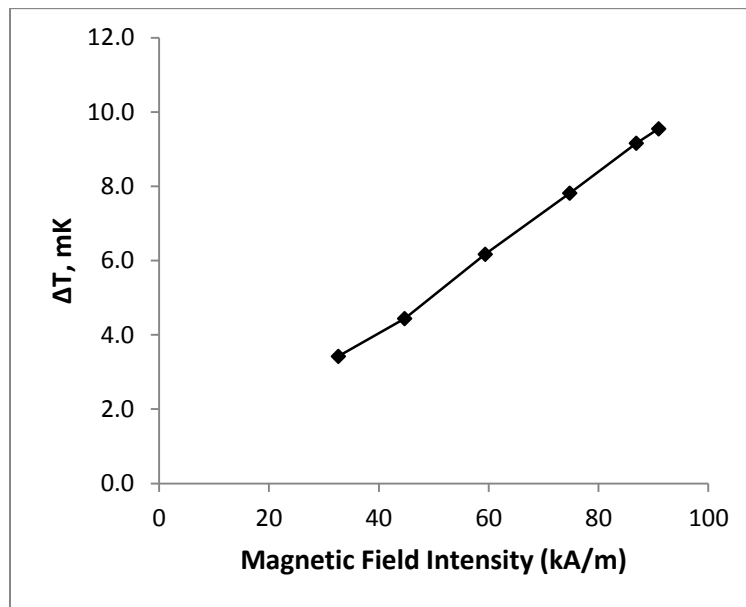
Figure 19. Monolithic Terfenol-D's change in temperature
with applied field. The data is obtained from Figure 16

5.2 Strain and DIC Results

Strain data from magnetostriction using the strain gage is shown in Figure 21. The applied field ranged from 0 to 127 kA/m with a maximum magnetostriction of about 770$\mu\varepsilon$. From this graph we can see the presence of hysteresis. In addition the magnetostrictive response did not show signs of saturation at this range of applied field.

32

DIC showed that a uniform x-displacement was exhibited throughout the material in Figure 20. The measurements were performed with respect to the center of the sample where the bar was held in place by the notches. Measurements for the Y-displacement were much less uniform which could be attributed to the mounting of the sample or the boundary conditions. Both the principle strains showed a random scattering of stresses. The strain measurement from this image was taken from the X-displacement image where the magnitude of displacement was divided by the sample length and resulted in a strain of $839\mu\varepsilon$. This strain value is plotted in Figure 21 as a single dot with the strain gage data. The DIC results and strain showed good correlation to each other and suggest that the strain measurements in the Terfenol D were consistent.

A noticeable difference when comparing both DIC and TSA is the information that can be shown. The information that can extracted from DIC are displacement values and in this case, the X-Y displacements. The principles strains however show a large variability in strain distribution. The TSA information given is the sum of principle strains so displacement information cannot be extracted. However, it appears that TSA can detect material effects that cannot be seen otherwise using DIC.
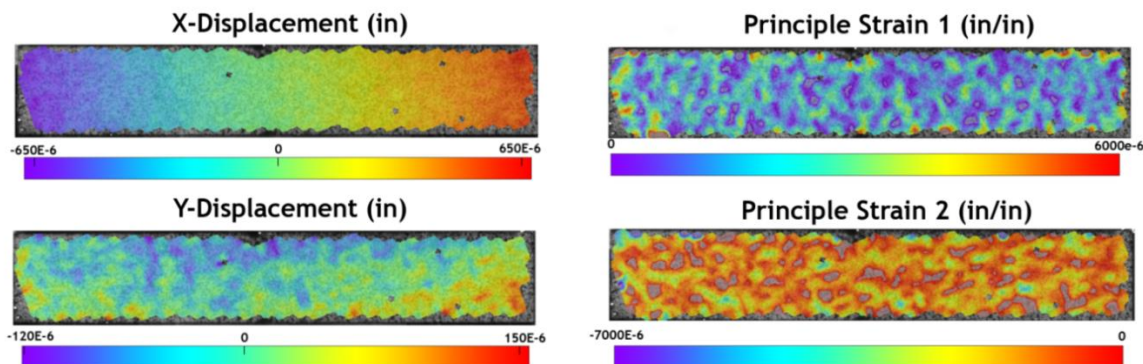

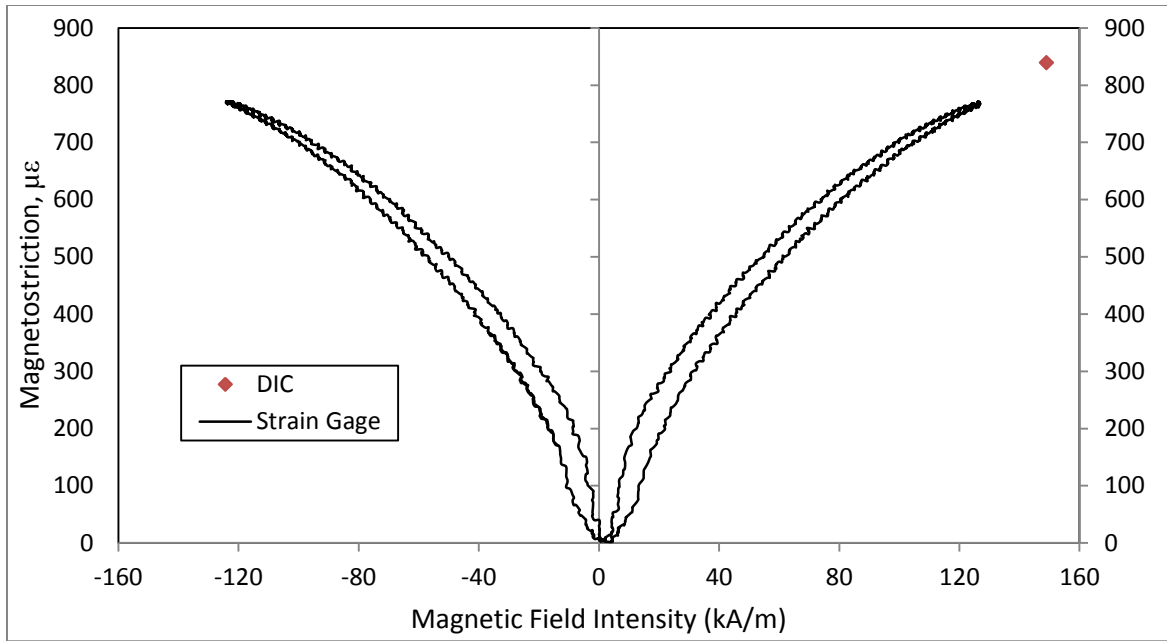Figure 20. DIC results for TML at magnetic field of 149 kA/m.

33

Figure 21. Magnetostriction response of TML using strain gage and DIC.

5.4 Finite Element Simulation Results

FEA results from the ANSYS simulation is shown in Figure 22 and Figure 23. The quarter model results were expanded by mirroring it about its symmetrical axes. The analysis was performed at 45, 75 and 92 kA/m for the large notched Terfenol D and 45, 75, and 87 kA/m for the smaller notchless one. This variation in magnetic field was to match that of the actual experimental data. The results displayed are the summation of principle strains. The profile shows similar distribution pattern to that of the thermal images. The strain is less at the two ends and much greater on the top and bottom edge. For the sample with the notches engraved in it, the location with the greatest strain was around the notched area. In the sample without notches, the strain was relatively uniform throughout the part. Note that the scale in Figure 22 is reduced to reveal the strain throughout the model since the fluctuations of the strain near the notches was much greater.

34
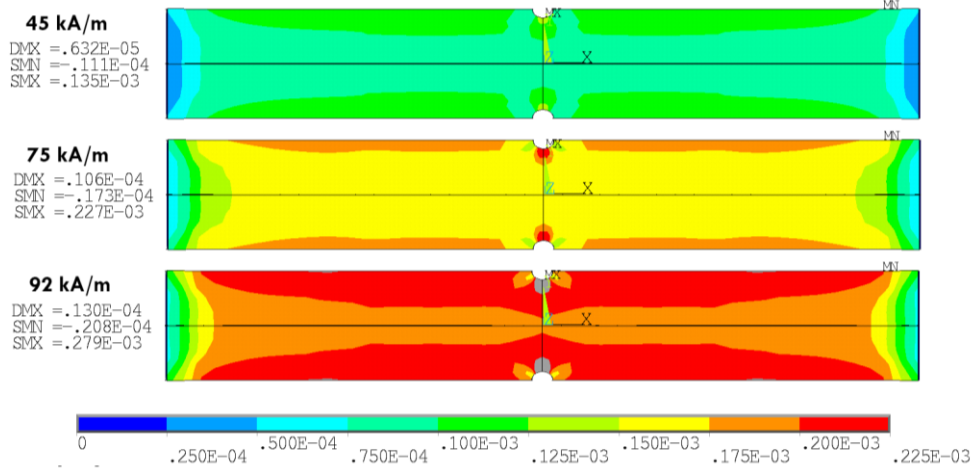
Figure 22. Summation of principle strains at different magnetic field
intensity for sample with notch, TML.

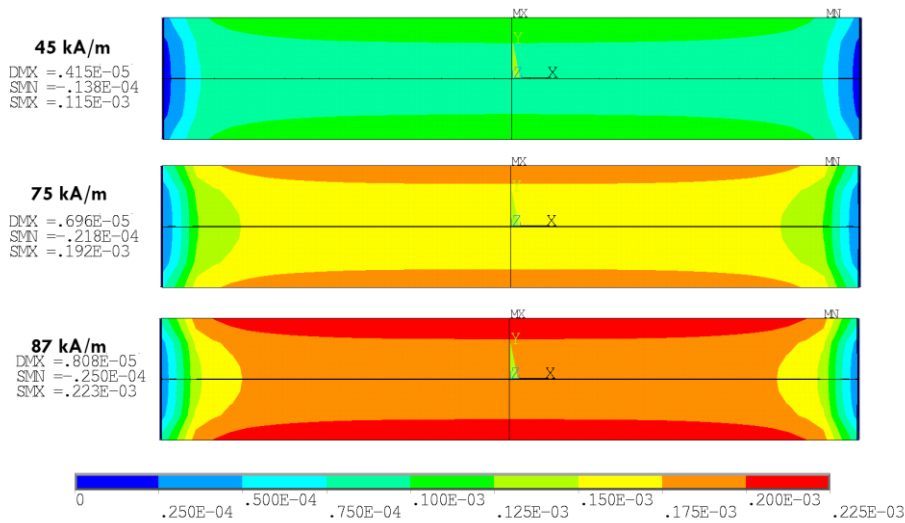Figure 23. Summation of principle strains at different magnetic field
intensity for sample without notch, TMS.

6. TERFENOL-D COMPOSITE RESULTS

During the periodic magnetic field cycling, only the TE0 and TE90 samples showed significate temperature changes. The TER sample did not produce any changes that were noticeable. The aligned particles did show variations in surface temperature as shown in Figure

24. However, the detected change in temperature was much smaller than that of the monolithic Terfenol.
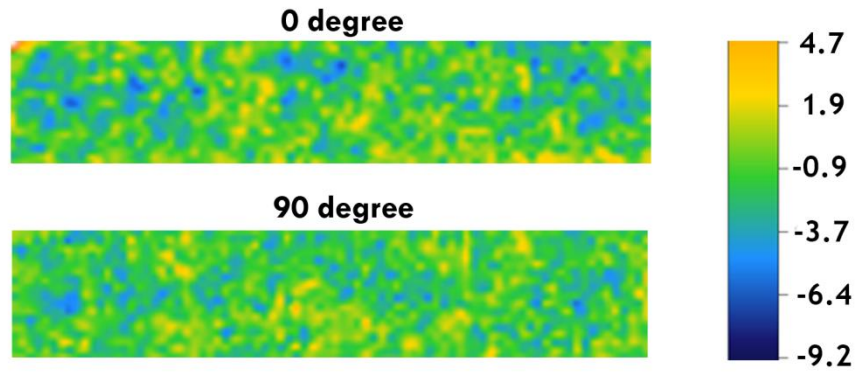
Figure 24. Temperature change of samples TE0 and TE90 at magnetic field of 95 kA/m. Temperature scale is in milliKelvins.

The thermal images shown were very non uniform and no clear signs of a trend or gradient were found. However, when we overlayed the microstructural images from Figure 10 ontop of those in Figure 24, the thermal images became more meaningful as shown in Figure 25. Terfenol-D particles are displayed as black specks on the thermal images in Figure 25. The regions of blue corresponds to little to no temperature activity from the particles. Regions of yellow showed high temperature activities. The number of particles present in the location played a key role in this. The blue regions generally contained little amount to almost no particles whereas the yellow region contained much more particles.
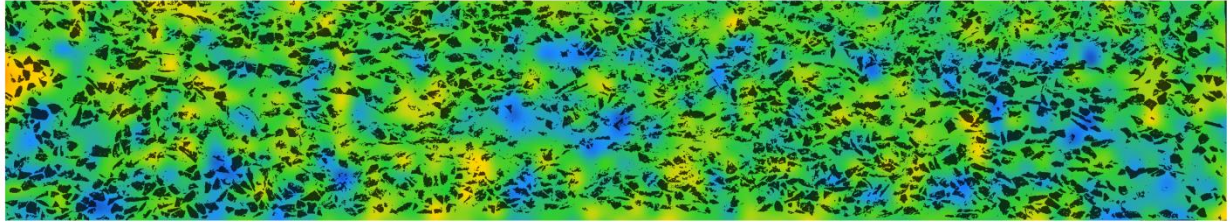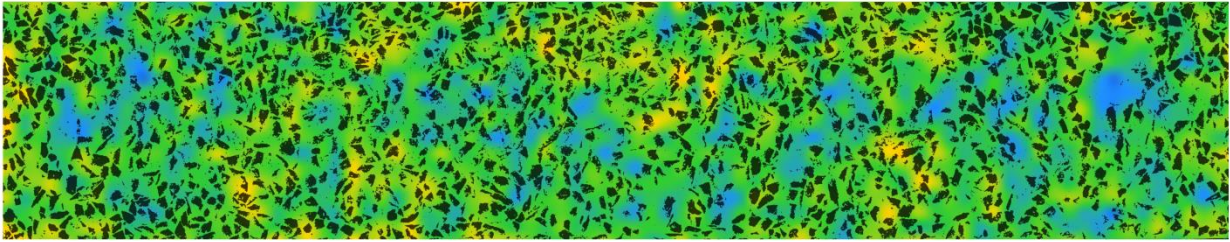
Figure 25. Overlay of Terfenol-D particles from Figure 10 over thermal images at 95 kA/m.

7. DISCUSSION

The thermal images from phase sensitive thermography revealed that there were temperature changes from periodic magnetization of the monolithic Terfenol-D and its composite form. In monolithic samples, these temperature changes were positive and increased with rising magnetic field intensity. The net strain associated with this magnetostriction ranged from 0 to positive 680 με. According to thermoelasticity, the change in temperature seen should have been decreasing with positive strain. However, the acquired thermal images showed the opposite effect. Thus it can be postulated that the observed positive thermal energy is attributed to the magnetocaloric effect. In fact, the coupling of thermoelastic and magnetocaloric was been proposed by Tishin and observed by Castello-Villa et al. in shape memory alloys [30, 56]. The location with higher summation of principle strains had more magnetic particles that were aligning with the easy axis. To compensate for entropy, more heat was released at these locations. This was further supported by the FEA model which showed that geometrically, the

37

edges of a rectangular sample experiences more magnetostrictive strain thus more heat was generated at these locations. In addition, other geometrical features, such as notches, producing large strains were also detectable.

The MCE of Terfenol-D has not been study extensively in literature so little information about MCE in this material was known as to whether it was operating near or away from its optimal magnetocaloric temperature range. However, terbium and dysprosium alloys containing relatively similar compositions have been studied by Nikitin et al [57]. The study revealed that $Te_{0.25}Dy_{0.75}$ yields a peak MCE occurring at 194K with a maximum temperature change of about 0.7K. In a study conducted by Tereshina et al., the addition of iron into TeDyHoCo increased the temperature of MCE from about 140K to 280K, closer to room temperature [58]. The addition of iron also reduced the maximum temperature change from 1.75K down to 0.5K. From these two studies, it can be said that the addition of iron into the $Te_{0.25}Dy_{0.75}$ will increase the temperature of peak MCE and reduce the maximum change of temperature down to within the range measured in this study. This may also shine light as to why MCE in this material have not been studied since ordinary thermography techniques may not be sensitive enough to measure this small temperature change [59].

Phase sensitive thermography on composites indicated that localized strains were present and that these strains occurred at locations where Terfenol-D particles were present. The observed temperature change however revealed no clear signs as to whether a composite sample was aligned or not. The cooler temperature also suggested that the resin rich areas experienced either tensile or no stress which may be related to residual stresses during that are relieved under magnetostriction. In addition, there is the possibility that the effects of thermoelasticity and magnetocaloric may cancel out one another through internal conduction [30]. For example,

38

particles in an area with many particles undergo magnetocaloric heating during magnetostriction. The interaction of several particles in the region would cause the surrounding epoxy to experience an overall positive stress leading to a reduction in temperature from thermoelasticity. The heat from the particles is conducted to the epoxy thus attenuating the overall thermal response. This may explain as to why the randomly orientated composite sample did not exhibit any noticeable temperature changes. When compared to the aligned particles, the randomly distributed particle samples may be experiencing varying stress intensities that cancelled each other in the resin areas due to the interactions of the unaligned particles. However, in aligned particles, the resin areas may be subjected to more intense stress caused by a group particles acting in unison like that of a single chain fiber.

The localized thermal detection of the composite samples suggests that the detection of microstructural effects in a monolithic sample is possible. The monolithic Terfenol-D tests showed that material variability were present. To demonstrate that these variabilities were of material itself and not from other sources, we performed two follow up tests. First, the monolithic sample was rotated 180 degrees and then placed back into the clamp and into the magnets where the test was performed. This rotation was to remove any sources of bias introduced by the clamp, magnetic field, and camera. Second, the black paint was carefully removed and reapplied to make sure that the artifacts were not caused by sample preparation. The test was then repeated again followed by the sample rotation.

Figure 26 and Figure 27 was the results of this follow up test for both the large and small monolithic sample, respectively. In these figures, the top row is the sample before the paint was removed. The circled artifact in the image showed a region towards the right where the temperature was lower compared to its surrounding areas. After rotating the sample 180 degrees

39

and repeating the periodic magnetization, the artifact still existed but is on the left side due to the rotation. The bottom row of images showed the sample after the paint layer has be removed and reapplied. Again, the artifacts were still present even after repainting the surface. For Figure 27, there is a circled region that shows discontinuity on the sample. Again, by following the procedure as before, the sample revealed no changes in thermal imaging. Visual inspection of the surface under a microscope also revealed no abnormal defects in the material surface at these locations.
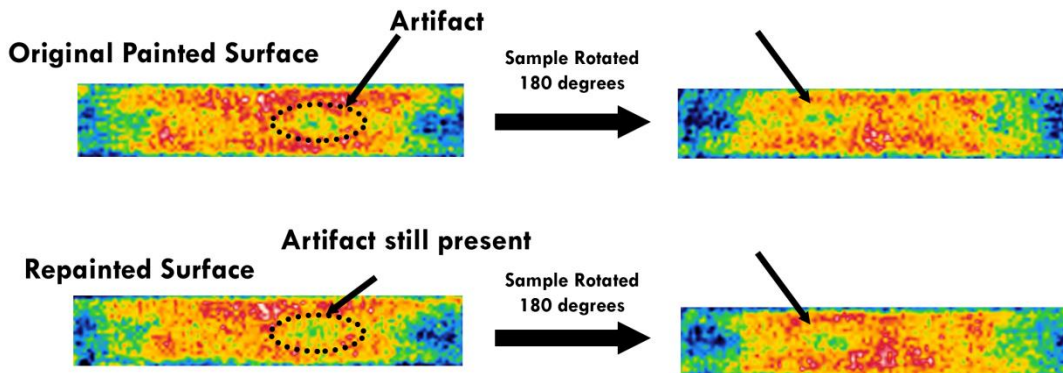

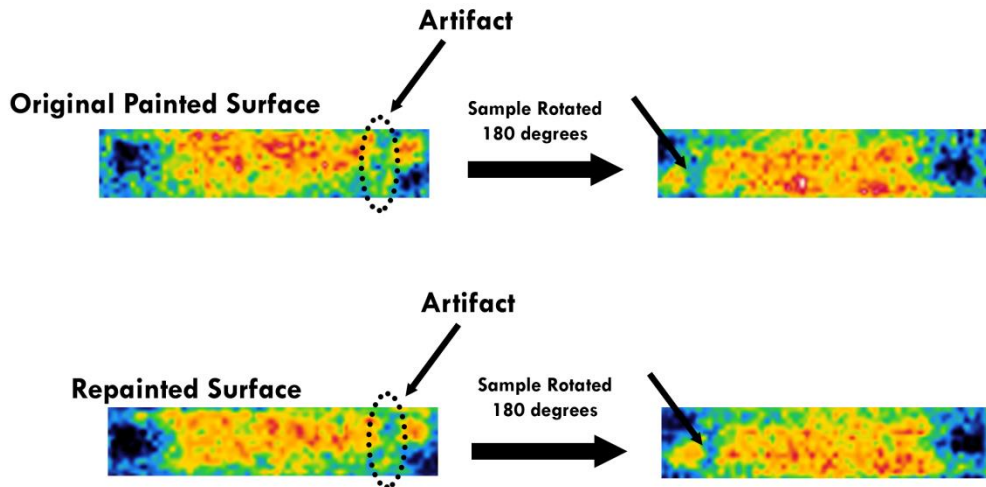Figure 26. Follow-up test results for large monolithic sample revealing artifacts.

Figure 27. Follow up test results for small monolithic sample revealing artifacts.

Thermography on magnetostrictive material that was limited by the fact that the temperature from thermoelastic stresses and MCE are indistinguishable. For example, a magnetic

field and negative or compressive stress applied together onto a magnetostrictive sample may have an additive effect on the change in temperature if both are in-phase with the same frequnecy. This was observed in initial trials but not presented in this study since applying both a known compressive stress and magnetic field in phase with each other requires a complex test setup which was not available. Another situation would be if the material is in a blocked setup where the material is restricted from magnetostriction producing compressive stress and while MCE occurs with magnetostriction.

8. CONCLUSION

In this study, phase sensitive thermography is used to examine the thermal effects associated with magnetostriction. To the best of our knowledge, we have observed MCE in T-D with phase sensitive thermography for the first time. We have demonstrated the superb sensitivity of this method for detection of MCE and thermoelastic effect. Test data show the ability to reveal and interrogate the microstructural inhomogeneity of the material from surface measurements. The ability to assess through the thickness defects will have to be investigated in future studies. In composites, it is able to measure the thermoelastic stresses from the interaction between the polymer matrix and the magnetostrictive material. There are other probable thermoelastic sources of heat, such as magnetic attraction of Terfenol-D particles causing the variation of strain in the matrix. However, the thermal effect was not seen in the FE control sample, i.e. the contribution from magnetic attraction is likely to be very small. Future tests may be able to quantify this effect. With the contribution from this effect eliminated, both magnetostriction and MCE should be the predominant factors. LT will be beneficial for quality assessment and design verification of composite transducers. In monolithic materials, it has the

41

potential to show uniformity of the material. Since the Terfenol-D used in this study is a polycrystalline, it is likely that the variability in the detected temperature is related to its crystal structure. The cause may be a combination of the mechanical interaction between the crystal structures in different orientations (thermoelastic) and their individual counterparts (magnetocaloric).

The observed temperature changes in the thermal images are combinations of the principal strains and are shown to be sensitive to geometry shape. In the finite element model of a rectangular sample, the strain is greatest near the edges that run parallel to the applied magnetic field. Other geometrical features such as notches will affect the strain distribution producing a rise in temperature. The temperature and strain distribution will be expected to be more uniform in a cylindrical sample. This study did not utilize cylindrical samples because the curved surface can distort the thermal readings.

This research has only scratched the surface on the potential of applying infrared thermography to magnetostrictive materials. This technology can be used to further understand the mechanism and interactions of magnetostriction, MCE, and thermoelastic effect. These initial findings indicate that the coupling of these effects exists. However, much work is still needed in terms of determining the extent of these couplings.

REFERENCES

1.   Ashley, S., *Magnetostrictive actuators*. 1998: Mechanical Engineering. **120**(6). pp.68-70.

2.   Goodfriend, M.J. and K.M. Shoop, *Adaptive characteristics of the magnetostrictive alloy, Terfenol-D, for active vibration control*. 1992: Journal of Intelligent Material Systems and Structures. **3**(2). pp. 245-254.

3.   Fenn, R.C., et al., *Terfenol-D driven flaps for helicopter vibration reduction*. 1996: Smart Material Structures. **3**. pp. 49-57.

4.   Zhao, X. and D.G. Lord, *Application of the Villari effect to electric power harvesting*. 2006: Journal of Applied Physics. **99**(8). pp. 08M703-08M703-3.

5.   Ekreem, N.B., et al., *An overview on magnetostriction, its use and methods to measure these properties*. 2007: Journal of Materials Processing Technology. **191**(1). pp. 96-101.

6.   Chiue, J.Y., H.P. Lin, and J.-C. Kuo, *Application of digital image correlation (DIC) on magnetostriction of Fe-Pd alloy*. 2012: Materials Science Forum 706-709. pp.1937-1942.

7.   Elhajjar, R.F. and C.T. Law, *Magnetomechanical local-global effects in magnetostrictive composite materials*. 2015: Modeling and Simulation in Materials Science and Engineering. **23**(7). pp. 1-13.

8.   Greene, R.J., E.A. Patterson, and R.E. Rowlands, *Thermoelastic Stress Analysis*, in *Handbook of Experimental Solid Mechanics*, W.N. Sharpe, Editor. 2008, Springer. pp. 743-763.

9.   Olabi, A.G. and A. Grunwald, *Design and application of magnetostrictive materials*. 2008: Materials and Design. **29**(2). pp. 469-483

10.   Moffett, M.B., et al., *Characterization of Terfenol-D for Magnetostrictive Transducers*. 1991: Journal of Accoustical Society of America. **89.** pp. 1448-1455.

11.   Clark, A.E., *Magnetostriction Rare-Earth-Fe2 Compounds*, in *Ferromagnetic Materials*. 1980: North-Holland, Amsterdam. pp. 531-589.

12.   Clark, A.E., H.T. Savage, and M.L. Spano, *Effect of stress on the magnetostriction and magnetization of single crystal Tb0.27Dy0.73Fe2* 1984: IEEE Transaction on Magnetics. **20**(5). pp. 1443-1445.

13.   *Galfenol*. 2015: Etrema [cited 2015 November]; Available from: www.etrema.com/galfenol/.

14.   *Terfenol D*. 2015: Etrema [cited 2015 November]; Available from: www.etrema.com/terfenol-d/.

15. Summers, E.M., et al., *Magnetic and mechanical properties of polycrystalline Galfenol*. 2004: Ames Laboratory Conference Paper, Posters, and Presentations. Paper 59.

16. Jiles, D.C. and J.B. Thoelke, *Theoretical modeling of the effects of anisotrophy and stress on the magnetization and magnetostriction of TbDyFe*. 1994: Journal of magnetism and magnetic materials. **134**(1). pp. 143-160

17. Teter, J.P., A.E. Clark, and O.D. McMasters, *Anisotropic magnetostriction in Tb0.27Dy0.73Fe1.95*. 1987: Journal of Applied Physics. **61**. pp. 3787-3789.

18. Kellogg, R. and A. Flatau, *Experimental Investigation of Terfenol-D's Elastic Modulus*. 2008: Journal of Intelligent Material Systems and Structures. **19**(5). pp. 583-595.

19. Tilly, R.J.D., *Understanding Solids, The Science of Materials 2nd Ed.* 2013, Southern Gate, Chichester, West Sussex, PO19 8SQ United Kingdom: John Wiley and Sons Ltd.

20. Engdahl, G., *Handbook of Giant Magnetostrictive Materials*. 2000, San Diego, CA 92101: Academic Press.

21. Calkins, F.T., M.J. Dapino, and A.B. Flatau, *Effect of prestress on the dynamic performance of a Terfenol-D transducer*, in *Smart Structures and Materials: Smart Structures and Integrated Systems*. 1997: San Diego, CA.

22. Liu, J., et al., *Magnetostriction under high presstress in Fe81Ga19 crystal*. 2010: Journal of Applied Physics. **108**(3). pp. 033913-033913-6.

23. Liang, Y. and X. Zheng, *Experimental researches on magneto-thermo-mechanical characterization of Terfenol-D*. 2007: Acta Mechanica Solida Sinica. **20**(4). pp. 283-288.

24. Kendall, D. and A.R. Piercy, *The frequency dependence of eddy current losses in Terfenol-D*. 1993: Journal of Applied Science. **73**(10). pp. 6174-6176.

25. Wan, Y., J. Qiu, and Z. Zhong, *Interfacial stiffness dependence of the effective magnetostriction of particulate magnetostrictive composites*. 2007: International Journal of Solids and Structures. **44**(1). pp. 18-33.

26. Dobrzanski, L.A., A. Wydrznska, and O. Lesenchuk, *Intelligent epoxy matrix composite materials consisting of Tb0.3Dy0.7Fe1.9 magnetostrictive particulates* 2009: Archives of Materials Science and Engineering. **35**(1). pp. 33-38.

27. Sandlund, L., et al., *Magnetostriction, elastic moduli, and coupling factors of composite Terfenol-D*. 1994: Journal of Applied Sciences. **75**. pp. 5656-5658.

28. Dobrzanski, L.A., et al., *Polymer matrix composite materials reinforced by Tb0.3Dy0.7Fe1.9 magnetostrictive particles*. 2009: Journal of Achievements in Materials and Manufacturing Engineering. **37**(1). pp. 16-23.

29. Warburg, E., *Magnetische untersuchungen*. 1881: Annalen der Physik. pp. 141-164.

30. Tishin, A.M. and Y.I. Spichkin, *The Magneteocaloric Effect and Its Applications*. Series in Condensed Matter Physics, ed. J.M.D. Coey, D.R. Tilley, and D.R. Vij. 2003: Institute of Physics Publishing.

31. Gomez, J.R., et al., *Magnetocaloric effect: A review of the thermodynamic cycles in magnetic refrigeration*. 2013: Renewable and Sustainable Energy Reviews. **17**. pp. 74-82

32. Pecharsky, V.K. and K.A. Gschneidner Jr., *The giant magnetocaloric effect in Gd5(SiXGe1-X)4 materials for magnetic refrigeration*. 1998: Advances in Cryogenic Engineering. **43**. pp. 1728-1736.

33. Gschneidner Jr., K.A., *The magnetocaloric effect, magnetic refrigeration and ductile intermetallic compounds*. 2009: Acta Materialia. **57**(1). pp. 18-28.

34. Tarin, M. and R. Rotolante, *NDT in composite materials with flash, transient, and lock-in thermography*, in *FLIR Technical Series*. 2011: Flir Systems, Inc: www.flir.com.

35. Andonova, A., *Comparison of transient thermography methods for defect detecting in electronic components and modules*. 2013 Proceedings of the 2013 International Conference on Electronics, Signal Processing and Communication Systems. pp. 118-122.

36. Wrobel, G., et al., *The application of transient thermography for the thermal characterisation of carbon fibre/epoxy composites*. 2009: Journal of Achievements in Materials and Manufacturing Engineering. **36**(1) . p. 49-56.

37. Breitenstein, O., W. Warta, and M. Langenkamp, *Lock-in Thermography: Basics and Use for Evaluating Electronic Devices and Materials*. 2nd ed, ed. K. Itoh, et al. 2010: Springer.

38. Redjimi, A., et al., *Noise equivalent temperature difference model for thermal imagers, calculations and analysis*. 2014: Scientific Technical Review. **64**(2). pp. 42-49

39. Breitenstein, O., et al., *Microscopic lock-in thermography investigation of leakage sites in integrated circuits*. 2000: Review of Scientific Instruments. **71**. pp. 4155-4160.

40. *What is a lock-in amplifier*, in *Technical Note TN1000*. 2000: PerkinElmer Instruments.

41. Wu, D., et al., *Applications of phase sensitive thermography for nondestructive evaluation*. 1994: Journal De Physique IV. pp. C7-567-C7-570.

42. Meola, C., et al., *Non-destructive evaluation of aerospace materials with lock-in thermography*. 2006: Engineering Failure Analysis. **13**(3). pp. 380-388.

43. Huth, S., et al., *Lock-in IR-Thermography - a novel tool for material and device characterization*. 2002: Solid State Phenomena. **82-84**. pp. 741-746.

45

44. Haj-Ali, R. and R. Elhajjar, *An infrared thermoelastic stress analysis investigation of single lap shear joints in continuous and woven carbon/fiber epoxy composites*. 2014: International Journal of Adhesion & Adhesives. **48**. pp. 210-216.

45. Lubarda, V.A., *On thermodynamic potential in linear thermoelasticity*. 2004: International Journal of Solids and Structures. **41**(26). pp. 7377-7398.

46. Pitarresi, G. and E.A. Patterson, *A review of the general theory of thermoelastic stress analysis*. 2003: The Journal of Strain Analysis for Engineering Design. **38**(5). pp. 405-417.

47. Quinn, S. and J.M. Dulieu-Barton, *Identification of the sources of non-adiabatic behavior for practical thermoelastic stress analysis*. 2002: The Journal of Strain Analysis for Engineering Design. **37**(1). pp. 59-71.

48. Offermann, S., et al., *Thermoelastic stress analysis under nonadiabatic conditions*. 1997: Experimental Mechanics. **37**(4). pp. 409-413.

49. Barone, S. and E.A. Patterson, *Polymer coating as a strain witness in thermoelasticity*. 1998: The Journal of Strain Analysis for Engineering Design. **33**(3). pp. 223-232.

50. *68 Material Data Sheet*. 2015: Fair-Rite Products Corp. [cited 2015 December]; Available from: www.fair-rite.com/68-material-data-sheet/.

51. Rajic, N. and N. Street, *A performance comparison between cooled and uncooled infrared detectors for thermoelastic stress analysis*. 2014: Quantitative InfraRed Technology Journal. **11**(2). pp. 207-221

52. Rajic, N. and D. Rowlands, *Thermoelastic stress analysis with a compact low-cost microbolometer system*. 2013: Quantitative InfraRed Thermography Journal. **10**(2). pp. 135-158

53. *Microbolometer Thermoelastic Evaluation*. 2015: Australian Government Department of Defense, Science and Technology.

54. Rauch, B.J. and R.E. Rowlands, *Thermoelastic Stress Analysis*. Handbook on Experimental Mechanics, 2nd Ed., ed. A.S. Kobayashi. 1993: Bethel, CT 06801: Society for Experimental Mechanics.

55. Robinson, A.F., et al., *Paint coating characterization for thermoelastic stress analysis of metallic materials*. 2010: Measurement Science and Technology. **21**(8). pp. 1-11.

56. Castillo-Villa, P.O., et al., *Elastocaloric and magnetocaloric effects in Ni-Mn-Sn(Cu) shape-memory alloys*. 2013: Journal of Applied Physics. **113**(5). pp. 053506.

57. Nikitin, S.A., A.M. Tishin, and P.I. Leontev, *Magnetocaloric effect and refrigerant capacity of Tb-Dy alloys*. 1989: Physica Status Solidi. **113**(1). pp. K117-K121.

58.   Tereshina, I.S., et al., *Magnetocaloric effect in (Tb,Dy,R)(Co,Fe)2 (R=Ho,Er) multicomponent compounds.* 2011: Journal of Physics: Conference Series. **266**. 012077-1-012077-4.

59.   Christensen, D.V., et al., *Spatially resolved measurement of the magnetocaloric effect and the local magnetic field using thermography.* 2010: Journal of Applied Physics, **108.** pp. 063913-1-063913-4